Biomass Conversion and Biorefinery
https://doi.org/10.1007/s13399-024-05350-6

ORIGINAL ARTICLE

Penicillium oxalicum-mediated the green synthesis of silica nanoparticles: characterization and environmental applications

Hazem Elsayed Kaabo[1] · Ebrahim Saied[1] · Saad El-Din Hassan[1] · Hesham M. Mahdy[1] · Mahmoud H. Sultan[1]

Received: 2 November 2023 / Revised: 5 January 2024 / Accepted: 20 January 2024

Abstract

In terms of biocompatibility, environmental friendliness, scalability, and cost-effectiveness, green nanoparticle (NP) synthesis is a modern area of nanotechnology that performs better than physical and chemical methods. The utilization of endophytic *Penicillium oxalicum* for the biogenesis of silica nanoparticles is the goal of the current work. The structural and optical properties of the fungal produced silica nanoparticles were investigated utilizing transmission electron microscopy (TEM), fourier transform infrared spectroscopy (FTIR), x ray diffraction (XRD) and dynamic light scattering (DLS). All of the investigated parameters and their interactions were found to have a significant effect on the crystallite size, according to the results. The average diameter size of the biosynthesized SiO_2-NPs was ranged between 20 -50 nm. The size of the biosynthesized SiO_2-NPs was 28.7 nm, and their crystalline nature was confirmed by XRD, according to characterization results. A surface plasmon resonance spectrum of silica nanoparticles was obtained at 280 nm. Under UV light, Ribazol black b and Crystal violet dyes were photocatalytically degraded utilizing biosynthesized SiO_2 nanoparticles. The highest decolorization percentage of Crystal violet and Ribazol black b was 94.1% ± 1.2% and 85.1% ± 0.93%, respectively after 90 and 120 min, for both crystal violet and Ribazol black b of incubation at 50.0 mg mL^{-1} of SiO_2 nanoparticles. Furthermore, SiO_2-NPs were successfully used more than once for biodegradation and that was regarded as its efficacy. Silica nanoparticles were used to remove Co, Pb, Cd, and Zn with percentages of 99.9% ± 1.2%, 99.9% ± 1.3%, 99.9% ± 1.3%, and 99.4% ± 1.4%, respectively. The phytotoxicity test was investigated by using *Zea mays* L seed which the root length increases to (28 ± 0.35) and (21 ± 0.51) cm, respectively when subjected tothe treated CV and Ribazole black b effluent... In conclusion, endophytic *Penicillium oxalicum* was used to successfully biosynthesize SiO_2-NPs, which showed, phytotoxicity, heavy metal bioremediation, and photocatalytic activity against CV and Ribazol black b dye.

Keywords Cost-effectiveness · Endophytic *Penicillium oxalicum* · Nanotechnology · Photocatalytic activity · Silica nanoparticles

1 Introduction

Over the last decade, the biosynthesis of nanoparticles has garnered significant interest owing to their physicochemical characteristics, strong optical properties, easy synthesis, controllable shape, and size [1]. Nanobiotechnology is a promising field in photocatalytic and bioremediation applications because of the size- and shape-dependent properties of metal nanoparticles [2]. Due to the presence of reductase enzymes, plant extracts and microorganisms such as fungi and bacteria can reduce heavy metals to metal nanoparticles with a narrow size distribution [3]. Unlike chemical synthesis, the green synthesis of silica nanoparticles does not require the addition of toxic chemicals for the capping process. Because the

✉ Ebrahim Saied
hema_almassry2000@azhar.edu.eg

Hazem Elsayed Kaabo
Hazemkaabo@gmail.com

Saad El-Din Hassan
Saad.el-din.hassan@azhar.edu.eg

Hesham M. Mahdy
mahdyhesham@azhar.edu.eg

Mahmoud H. Sultan
prof.mahmoud@azhar.edu.eg

[1] Botany and Microbiology Department, Faculty of Science, Al-Azhar University, Nasr City 11884, Cairo, Egypt

Published online: 01 February 2024

proteins in the microbes function as capping and reducing agents, the method is more environmentally friendly [4]. The current research has been undertaken to explore the utilization of endophytic fungal extract for the synthesis of silica nanoparticles for the bioremediation of some heavy metals and the biodegradation of dyes. The textile industry produces a large volume of colored dye effluents, which are toxic and non-biodegradable [5]. About 60–70% of the various dyes used in the textile industry are azo compounds. These dyes release hazardous and possibly cancer-causing substances into the aqueous phase, which leads to serious environmental pollution issues [6]. Around the world, 748 million people lack access to clean drinking water. The requirement for water is expected to rise by 400% by 2050, which will make the situation worse [7]. Microorganisms, organic, inorganic, and heavy metal contaminants are the main causes of water pollution. Pesticides, dyes, and antibiotics are examples of organic pollutants [8]. Additionally, according to Nahiun et al. [11], sewage treatment facilities release 3 to 10 billion gallons of untreated waste each year. Different dyes, such as methyl orange, malachite green, and bromophenol blue, when released in significant amounts, severely pollute water reservoirs [13, 14]. The treatment of industrial wastewater sustainably has become quite difficult due to these pollutants. For the removal of contaminants from wastewater, a number of remedial procedures have already been utilized, including adsorption, flocculation, coagulation, physical and biological treatments, ozonation, chlorination, ozone, UV radiation, chemical oxidation, and an enhanced filtering process, among others [16, 17]. All of the aforementioned methods have significant drawbacks, such as secondary pollution production as a result of byproducts, incomplete degradation of pollutants that results in the production of additional hazardous materials, and low system efficiency. Photocatalysis is a promising option for resolving these issues since it uses an environmentally favorable technique and produces no secondary pollutants or waste [18, 19]. Nanomaterials may be used to filter water in two different ways, including the use of inexpensive nanoadsorbents and nanofiltration, to increase the efficacy of wastewater treatment procedures [20]. Due to their unique characteristics and important functions in water treatment facilities, nanoparticles have garnered a lot of interest over time. In comparison to other microorganisms like algae, yeast, or bacteria, the use of fungi as biocatalysts in the production of silica and other different nanoparticles offers several benefits. It is commonly known that fungi can biosynthesize NPs, particularly metal NPs [21]. The benefits of producing nanoparticles with fungi as opposed to other biological agents. These primarily include a high level of tolerance to heavy metals, ease of mass-culture fungal cultivation, extracellular nanoparticle synthesis that lowers downstream costs, etc. that are environmentally benign and commercially viable to cover a sizable area [22]. The positive charge that the metal ions possess attracts fungi, which starts the biosynthesis process. But metal ions also induce certain proteins, and these hydrolyze the ions. Different strains of fungi, including *Fusarium oxysporum*, *Penicillium crustosum*, *Fusarium solani* and *Agaricus bisporus*, among others, have been used to synthesize nanoparticles such as silica, palladium, gold and silver [23–26]. The advantages of silica include its low cost, safety, thermal stability, and chemical inertness. Additionally, its photocatalytic efficiency for destroying organic pollutants is higher than that of other metals. Furthermore, silica-based photocatalysts are created, such as those made of silica-alumina [30], silica-supported zirconia [31], silica-supported magnesia [32], and silica-alumina-titania [33], which have higher UV activity at room temperature. The authors really employed SiO_2 nanoparticles to keep the particles' structure and to stop them from aggregating during photocatalytic reactions [34]. When it comes to technical applications, nanosilica is one of the most significant inorganic substances. Nanosilica particles are employed extensively in the manufacturing, materials, and industrial sectors, as well as in the fields of medicine, electronics, and the environment [35]. The majority of researchers employ chemical and/or physical methods to produce silica nanoparticles, but they are increasingly attempting to replace these methods with the use of environmentally friendly solutions [36]. Advanced oxidation process (AOPs) systems with nanomaterial inclusion are a frequent method for treating wastewater. AOPs generate hydroxyl (OH) radicals, which are highly reactive and useful for treating wastewater. They can also create intermediate products with low toxicity, according to Nidheesh et al. [37]. The other beneficial properties of nanomaterials, such as their direct bandgap, layered structure, high optical absorption coefficient, and optimized catalysis because of their small band edges, help treat water by removing various pollutants and assisting groundwater purification [38, 39]. The current study focuses on the use of SiO_2 nanoparticles for the photodegradation of dyes. Crystal violet and Ribazol black b were chosen as the dyes because of their heterocyclic nature, which is toxic and can lead to respiratory problems, vomiting, hyperhidrosis, and mental health issues. Additionally, these dyes have been extensively utilized in the textile, food, paper, and leather sectors. This study is designed to test the produced SiO_2 nanoparticles for their photocatalytic activity in the destruction of CV and Ribazil black b under UV light irradiation. The

technique used was a relatively straightforward, low-cost, and economical way to create SiO_2 nanoparticles.

2 Materials and methods

All the chemicals, reagents, Czapex-Dox agar media (CDA), Czapex-Dox broth media (CDB), potato dextrose broth media, and sodium silicate were acquired from Sigma Aldrich and had a purity level of 99%. The precursor utilized was sodium silicate. In order to confirm the substance's photocatalytic characteristics, photodegradation operations on a few dyes were conducted. In this investigation, distilled water was used to complete every biological synthesis.

2.1 Isolation and identification of fungal strain mediated synthesis of NPs

The fungus *Penicillium* sp. was isolated from soil taken from Nasr City in Cairo, Egypt (GPS coordinates: N: 30°010 68.939″, E: 31°370 70.336″). Czapex Dox agar medium (CDA) mixed with antibacterial agents was used for the isolation process, and 1.0 mL of a 10^5 sample dilution was used as the inoculum (Fouda et al. [40]) (with minor modifications). The plate was incubated at 30 °C ± 2 for 48 h. The pure strain was identified morphologically, culturally, and molecularly using a standard key that was published by Pitt, [41] and Visagie, [42]. Additionally, microscopic features such as conidiophore branching, metulae and phialides structures, and conidia (shape and size) were meticulously measured. Phenotypic identification was confirmed by partial genotypic sequencing of the Internal Transcribed Spacer [43]. The fungal strain was employed for the green synthesis of SiO_2 nanoparticles, as stated in [23].

3 Nanoparticle synthesis

3.1 Preparation of fungal biomass filtrate

Penicillium sp. was inoculated into two disks (1.0 cm) and placed in 100 mL of potato dextrose broth medium. The mixture was then shaken at 150 rpm and cultured for 6.0 days at 30 °C ± 2 °C with a pH of 5. Following the incubation period, the fungal biomass was obtained by filtering it through Whatman Filter Paper No. 1 and rinsed three times with sterile distilled water to eliminate any medium components. 20 g of the collected fungal biomass were resuspended in 100 mL of sterile distilled water and shaken at 150 rpm for 72 h at room temperature. The prior combination was centrifuged to get the cell-free filtrate (biomass filtrate), which was then utilized to create NPs using a green process [44].

3.2 Green synthesis of SiO_2-NPs

The previously disclosed of technique El-Gazzar et al. [45] was followed, with a few modifications, for the biosynthesis of SiO_2-NPs. A 100 mM sodium silicate stock solution was made in order to perform the biosynthesis of SiO_2-NPs. In order to get the final concentration of 3.0 mM, 3.0 mL of the prior solution was then added to 97 mL of biomass filtrate. Using an orbital shaker at 150 rpm and no light, the solution was incubated at room temperature for 24 h. The color of the NP synthesis was observed. The created NPs were centrifuged at 10,000 rpm for 15 min, washed three times in distilled water, and then dried in an oven at 100 °C for 12 h. The resultant precipitation of silica nanoparticles was turbid-white and was collected. The sodium silicate solution and the biomass filtrate without any metal precursors were used as the experiment's controls.

3.3 Factors affecting nanoparticle synthesis

Using UV–Vis spectroscopy, a Jenway 6305 Spectrophotometer, (Jenway, Staffordshire, UK) was used to measure the maximum surface plasmon resonance, which allowed the investigation of the parameters influencing the synthesis and dispersion of NPs. These included pH values (3.0–10.0), time of contact between biomass filtrate and NPs precursors (12, 24, 36, 48 and 72 h), precursor (sodium silicate) concentrations (1.0–5.0 mM), and incubation temperature of the biomass filtrate and metal ions (25, 30, 35, and 40 °C). Incubation periods for fungal biomass in distilled water were also taken into consideration. On a nanoparticle that had its SPR value previously discovered, these variables were measured. The highest absorbance peaks at 280 nm for SiO_2-NPs were measured to determine the ideal circumstances.

3.4 Instrumental analysis of the optimized SiO_2-NPs.

The subsequent characterization techniques were used to ascertain the physical characteristics of the obtained post-biotransformation SiO_2-NPs under ideal circumstances. The form and size of the biosynthesized SiO_2-NPs were investigated using transmission electron microscope analysis (TEM) (JEOL 1010, Japan). The samples were made by drop-coating the SiO_2-NPs solution onto a copper grid that had been coated with carbon. The color shift caused by the production of NPs was observed using UV–Vis spectroscopy (JENWAY 6305 Spectrophotometer) at a wavelength of 200–800 nm. The crystallinity of biosynthesized SiO_2-NPs was further examined using XRD patterns on a Philips X'Pert Pro X-ray diffractometer (Eindhoven, Netherlands). The range of the 2θ was between 4° and 80°. The X-ray source was Cu-Ka radiation that had been

Ni-filtered. There was a 40 kV voltage and a 30 mA current. The Debye–Scherrer equation was used to determine the average size of NPs produced from the fungal metabolites [46]. Using DLS analysis, it was possible to determine the sizes and distribution of biosynthesized metal oxide NPs in colloidal solutions. The samples were reconstituted in distilled water before being measured by DLS using a Nano ZS Zeta Sizer (Malvern, UK). Through the measurement of the polydispersity index (PDI), DLS analysis can reveal information regarding the homogeneity of NP solutions [47]. Finally, using Fourier transform infrared (FTIR) Spectroscopy (Agilent System Cary 660 FTIR model), it was determined how fungal metabolites and various functional groups contributed to the reduction, capping, and stabilization of SiO_2-NPs. To produce FTIR spectra, the materials were scanned between 400 and 4000 cm^{-1} [48].

4 Catalytic activity against crystal violet (CV) and Ribazol black b dyes

In the presence of UV light, the ability of biofabricated SiO_2-NPs to break down CV and Ribazol black b as a dye model was studied. Each SiO_2-NPs concentration (30 and 50 mg L^{-1}) was independently added to the CV and Ribazol black b solution (50 mg L^{-1}) for a variety of contact periods (30, 60, 90, 120, and 150 min). The CV and Ribazol black b solutions were stirred at room temperature for 25 min prior to the experiment to achieve the equilibrium of absorption and desorption between the dye solutions and the surface of the nano-catalyst [49]. The effectiveness of each SiO_2-NPs concentration to adsorb or degrade the CV and Ribazol black b solutions was evaluated in comparison to the control (CV and Ribazol black b solutions without SiO_2-NPs separately) by mixing the nano-catalyst and the CV and Ribazol black b solutions under light settings with air bubble aeration. 2 mL of each treatment were taken out at regular intervals and centrifuged for 15 min at 3000 rpm. A crystal-clear supernatant was collected. The M-ETCAL spectrophotometer was then used to measure their optical density at a maximum λ max of CV and Ribazol black b solutions at 664 nm. The following equation was used to compute the percentages of color removal:

$$Decolorizationpercentages(\%) = D - D1/D \times 100 \quad (1)$$

where D is the initial absorbance and D1 is the final absorbance at interval times.

The trapping approach was used to look into the role that various reactive species, including hydroxyl radicals ($^{\bullet}OH$), superoxide radicals ($^{\bullet}O_2^-$), and holes (h^+), play in the breakdown of CV and Ribazol black b. In this procedure, reaction solutions containing 20 g mL^{-1} of green produced SiO_2-NPs to 10 mg L^{-1} of CV and Ribazol black b solution were added separately for 150 min under UV light irradiation at pH 7 the reaction solutions containing 1 mM of isopropyl alcohol (IPA), 1 mM of benzoquinone (QB), and 1 mM of ethylenediaminetetraacetate (EDTA). These substances, in turn, serve as quenchers for $^{\bullet}OH$, O_2^-, and h^+ [50]. Following the contact period, the mixture's absorbance was determined to be 664 nm, and the degradation percentages were then determined as previously described. To boost the dye adsorption even further, the catalyst's reusability was examined over the course of six cycles. The nano-catalyst was used in the second cycle after being retrieved from the first cycle and having undergone three washes with distilled water to eliminate any leftover water.

5 The in vitro heavy metals adsorption by SiO_2-NPs

Using a PerkinElmer Analyst 800 atomic spectrometer, the key common heavy metals in wastewater, including Hg, Co, Pb, Cd, and Ni, were evaluated both before and after NPs treatment. Atomic absorption spectroscopy relies on the free metallic ions' ability to absorb light to detect heavy metals. To test the silica nanoparticles ability to adsorb the selected metals, aquarium water was introduced with a metal concentration of 100 ppm. To assess the adsorption capacity of SiO_2-NPs, water samples were obtained after 24 h [51]. Atomic Absorption Spectrophotometer was carried out in the Faculty of Veterinary Medicine, Zagazig University, Egypt.

6 Phytotoxicity test

To investigate the phytotoxicity of CV and Ribazol black b solutions both before and after SiO_2-NPs treatment, maize seedlings (*Zea mays* L.) were employed. Healthy seeds were picked when purchasing the plant seeds from the neighborhood store. These healthy seeds underwent five rounds of sterile dist. H_2O washing after being submerged in 2.5% sodium hypochlorite for five minutes. They were then mixed with 70% ethanol for one minute. The treatments included using tap water as the control (A), CV and Ribazol black b solutions before any treatment (B), and CV and Ribazol black b solutions following the optimum conditions of SiO_2-NPs treatment for each dye (C and D), respectively. The chosen seeds were germinated in tap water before the experiment until 0.5 cm of radical seed emerged to verify the health of the seed. A Petri dish (diameter = 25 cm) containing filter papers was then filled with four groups, each of which contained five uniformly germinated seeds, and the groups were watered as necessary with the prior treatment. At 30 °C, the plates were incubated [52, 53]. After 16.0 days

of incubation, the growth metrics, including the shoot length and root length, were determined. Three duplicates of the experiment were performed.

6.1 Assessing the impact of CV and Ribazol Black b solutions on *Zea mays* growth: A greenhouse pot experiment before and after SiO_2-NPs treatment

In a fully randomized pot experiment, the growth performance of *Zea mays* L (Cultivar Giza 9) was examined to determine the toxic effectiveness of CV and Ribazol black b solutions before and after SiO_2-NPs treatment. Sandy soil was used for the greenhouse experiment; it had the following chemical and physical characteristics: P (21.6 mg kg^{-1}), K (14.9 mg kg^{-1}), Na (183.1 mg kg^{-1}), Ca (27.1 mg kg^{-1}), and Cl (127.2 mg kg^{-1}). Its texture was a mixture of sand (96.6%), silt (2.28%), and clay (1.13%). Positive control, negative control, and biodegradable materials (see seed germination section) were the treatments that were used. Prior to the experiment, *Zea mays* seeds were surface sterilized by soaking in sodium hypochlorite (2.5%) for 3 min and then being rinsed three times with distilled water. After that, three groups of comparable sterilized germination seeds were chosen by allowing the sterilized seeds to pre-germinate. Three germination seeds were placed in each of the five pots used in the experiment, five for each treatment. The preceding treatment was applied to the planting pots as needed, and they were incubated for 45 days at 25 to 30 degrees Celsius. The plant was collected at the conclusion of the experiment, the shoot and root systems were divided, and any soil fragments still connected to the root systems were removed. Calculations were made about the plant's height, root length, fresh weight, and dry weight of the shoot and root systems [54, 55].

7 Statistical analysis

Data collected in the present study are presented as the means of three independent replicates and subjected to statistical analysis using the statistical package SPSS v17. The mean difference comparison between the treatments was analyzed by t-test or the analysis of variance [56], and it was subsequently analyzed by the Tukey HSD test at $p < 0.05$.

8 Results and discussion

8.1 Potency of the fungal isolate for SiO_2-NPs biosynthesis

Out of 18 fungal isolates obtained, only one (no.13) appeared to biosynthesize SiO_2-NPs. This isolate no. 13 was identified

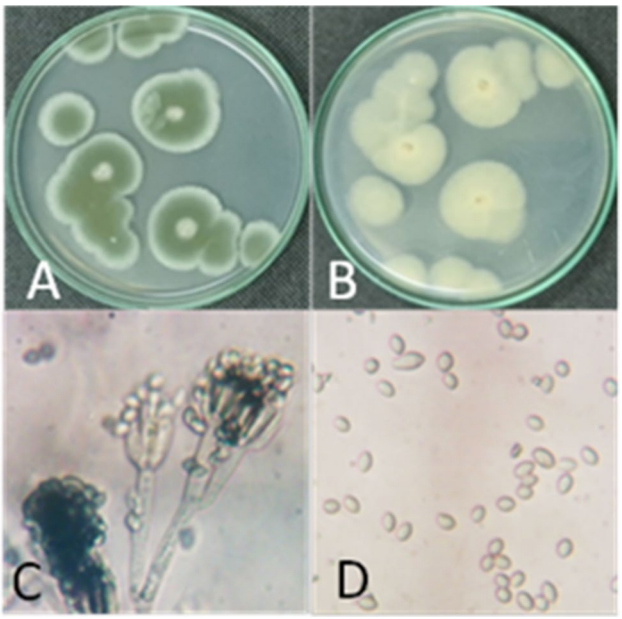

Fig. 1 Morphological examination of *Penicillium* sp.: A, B illustrating the surface and reverse color of fungal colony, C and D focusing on conidiophores branching, phialides and conidia (800× magnification)

at the genus level morphologically as *Penicillium* sp. The plate culture of the fungal isolate was initially examined and identified as *Penicillium* sp (Fig. 1). The growth rate of *Penicillium* sp on Czapex Dox agar (CDA) medium showed rapid progression, reaching 45 mm colony diameter in five days with a dark olive-green velvety colony surface, while the reverse color was creamy white. Using a light microscope, *Penicillium* sp. showed biverticillate branched conidiophores ended with ampulliform phialides bearing a series of smooth oval to ellipsoidal conidia.

The molecular identification was carried out for 18S-28S rRNA gene sequence. DNA was extracted from *Penicillium* sp (no. 13). The PCR test was carried out for the 18S-28S rRNA gene. The PCR product was electrophoresed on a 1% agarose gel and showed a DNA band of about 593 bp. The amplicon of the PCR 18S-28S rRNA product flanking ITS1, 2 and 5.8 S regions for *Penicillium* sp was sequenced (Supplementary Fig. S1). The sequence of the amplified ITS1 fragment (549 bp) was set down in the NCBI database. This sequence showed more than 99% homology with other sequences of related *Penicillium oxalicum* strains recorded in GenBank (MF135517, KU743897, OR229697, ON045456, KT354504, ON127863) and then recorded as *Penicillium oxalicum* strain MH-com with accession number OR617065. A phylogenetic tree (Fig. S1) based on the ITS1 region sequences with other reference *Penicillium* species recorded in the NCBI GenBank was created to investigate the phylogenetic relations of the strain under study. The

results showed that *P. oxalicum* OR617065 belongs to the *P. oxalicum* species with a bootstrap value of more than 99% and is in the same clade. This technique was used by Albalawi et al.[57], who mycosynthesized silica nanoparticles by using a biomass filtrate of *A. niger* AH1.

8.2 Green synthesis of silica nanoparticles (SiO_2-NPs).

Penicillium spp. have the ability to synthesize various NPs [58, 59]. In the fungal-based NP biosynthesis, intracellular and extracellular enzymes and biomolecules reduce various metal ions as part of the biomineralization process [60]. Through the process of intracellular synthesis, metal salt is added to the fungal culture, causing the biomass to produce and internalize nanoparticles. To disrupt the fungal biomass and extract the nanostructures, a variety of techniques are used, including centrifugation, filtration, and chemical treatment. In order to produce non-aggregating nanoparticles in the medium, the more popular extracellular approach entails combining the metal precursor with the fungal filtrate that contains the biomolecules [1, 61]. In this study, the biomass filtrate of the fungus strain *P. oxalicum* was used in this investigation as a catalyst to form SiO_2-NPs which enhance the production process, decrease the aggregation, and produce a smaller size [62]. As illustrated in Fig. 2, the biomass filtrate's color changed after it was combined with metal precursors, marking the first observation regarding the biosynthesis of NPs. The synthesis of silica nanoparticles, which were calcined at 100 °C to form SiO_2-NPs powder, caused the color to change to turbid-white as a result. In order to successfully biofabricate of silica nanoparticles, Albalawi et al. [57] used the *Aspergillus niger*. Huang et al. [63] comparing the green synthesized nanoparticles method with reducing agent coating to traditional physical and chemical methods reveals an intriguing and multifaceted application. On the other hand, Huang et al. [64] success to synthesize of bimetallic nanocomposites Ag with nickel and cobalt by using the extract of *W. coagulans.* Furthermore, Hussain et al. [65] synthesize ZnO NPs using the natural plant extract of *Fagonia cretica.*

8.3 Optimization of the physiochemical parameters for SiO_2-NPs biosynthesis

The optimization of the biosynthetic factors, such as reaction durations, incubation temperatures, pH, and various salt concentrations, was explored in an effort to improve size control. Each parameter was changed one at a time, while the other test circumstances remained constant. The presence of a significant quantity of silica in a relatively limited volume of the salt solution may be the cause of

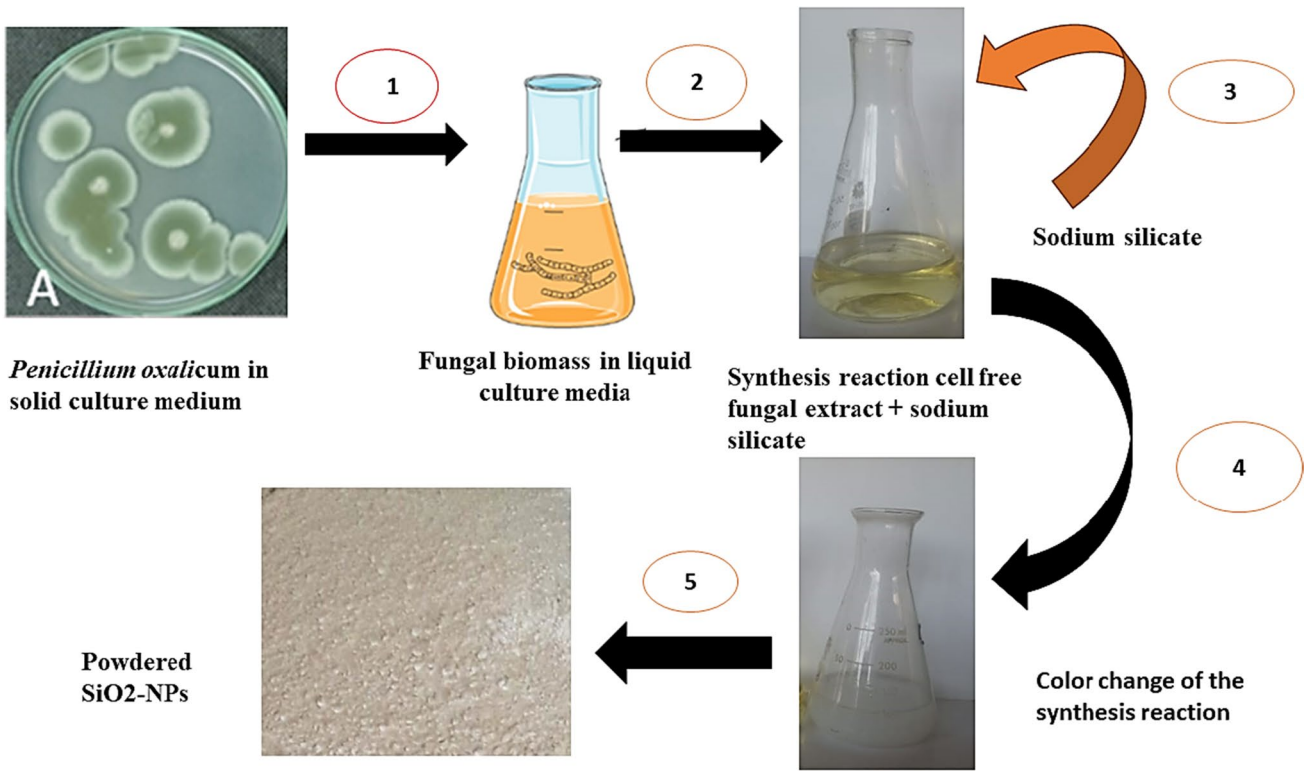

Fig. 2 Extracellular biosynthesis of SiO_2-NPs by using endophytic *Penicillium oxalicum*

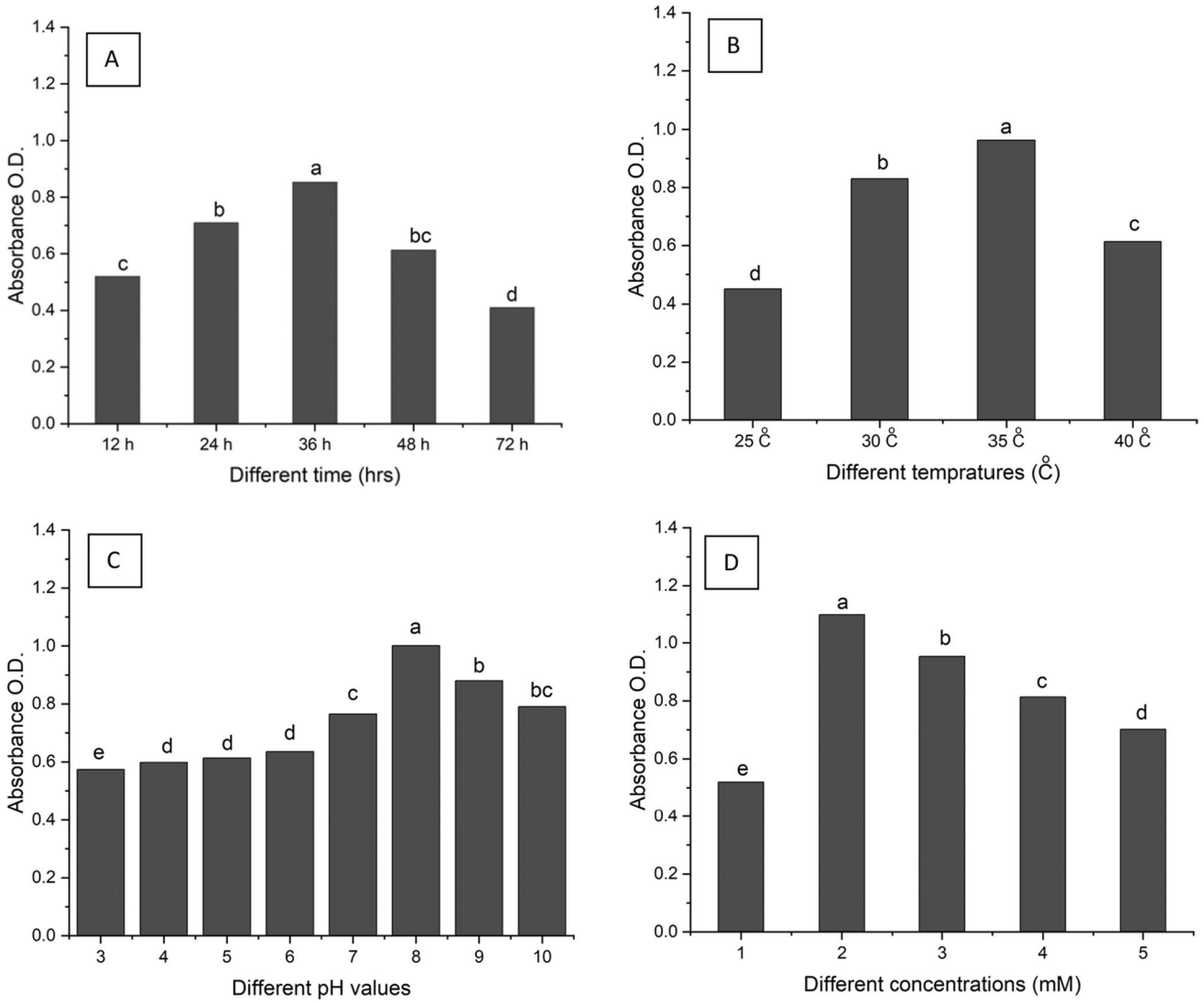

Fig. 3 Optimizing factors for biogenic SiO_2-NPs using *Penicillium oxalicum*, (**A**) denotes the contact time between biomass filtrate and optimum sodium silicate concentration.; (**B**) denotes the effect of incubation temperatures on biogenic SiO_2-NPs.; (**C**) illustrates the effect of pH values, and (D) denotes the different sodium silicate concentrations

the formation of large particles. The amount of hydrogen ions present in the reaction medium is a key factor in NP size determination. Similar to the current findings, Abd Elmohsen et al. [66] showed that the enzymes released by the fungus alter their catalytic activity as the pH of the reaction mixture varies. Due to the release of more of the reducing agent necessary for NPs production as fungal biomass grew [57], the biosynthesis of SiO_2-NPs increased. Increases in fungal biomass resulted in smaller nanoparticles as well as faster reactions, which may have been caused by the abundance of fungal enzymes. In this study, the effects of incubation duration, pH, temperatures, and various fungal filtrate and precursor concentrations were examined. The information showed that 36 h was the ideal incubation time for the production of bioactive compounds. Before or after that time, lower NP synthesis was observed (Fig. 3 A). The size and form of NPs are also influenced by the solution's color intensity, which is a function of the contact time [67]. The wavelength and absorbance peak dropped when the contact duration was increased further because NPs tended to agglomerate [68]. According to the information in Fig. 3 B, 35 °C was the ideal temperature for the biosynthesis of SiO_2-NPs. Up to a temperature of 35 °C, the formation was accelerated, but temperatures above that reduced biosynthesis. According to Albalawi et al. [57], *A. niger* AH1 biomass filtrate was used to mycosynthesize SiO_2-NPs, which were then incubated at 25 °C for an overnight period. In contrast, the SiO_2-NPs produced using ethanolic green tea leaf extract were rinsed with ethanol and water before being vacuum-dried at 50 °C overnight [69].

Additionally, Ramya et al. [69] reported that the SiO_2-NPs were produced by calcining HCl-treated rice husk at 700 °C for two hours in a muffle furnace. The SiO_2 nanoparticles were over-dried (80 °C) for 24 h and then calcined in the furnace at 500 °C for 3 h [70]. The findings in Fig. 3 C; demonstrate how the biosynthesis of SiO_2-NPs is affected by various pH levels between 3 and 10. The best conditions for the production of NPs were alkaline. At maximal absorbance, SiO_2-NPs were most productive when the pH was 8.0. According to Cai et al. [71], an alkaline pH was necessary for Fe_3O_4@SiO_2 nanoparticle production. The production of NPs was enabled by the fact that the reducing capability of the functional groups engaged in the biomass filtrate was inhibited in an acidic environment and elevated in an alkaline environment [72]. According to Sidhu et al. [4], varying pH levels can alter the charge on biomolecules, which in turn affects how efficient they are as capping and stabilizing agents. The concentrations of the precursors have an impact on SiO_2-NP biosynthesis as well. Investigations were conducted using sodium silicate concentrations ranging from 1.0 to 5.0 mM (Fig. 3 E). In the present investigation, increasing precursor doses up to 2.0 mM enhanced the absorbance at λ 280 for SiO_2-NPs. The great effectiveness of the proteins and enzymes found in biomass filtrate in decreasing the precursors at these concentrations may be credited with this discovery [73]. Because NPs have a tendency to cluster or agglomerate at higher precursor concentrations, their absorbance was reduced [46]. *A. niger* AH1 biomass filtrate was used by Albalawi et al. [57] to biosynthesize SiO_2-NPs in a 4 M sodium silicate solution.

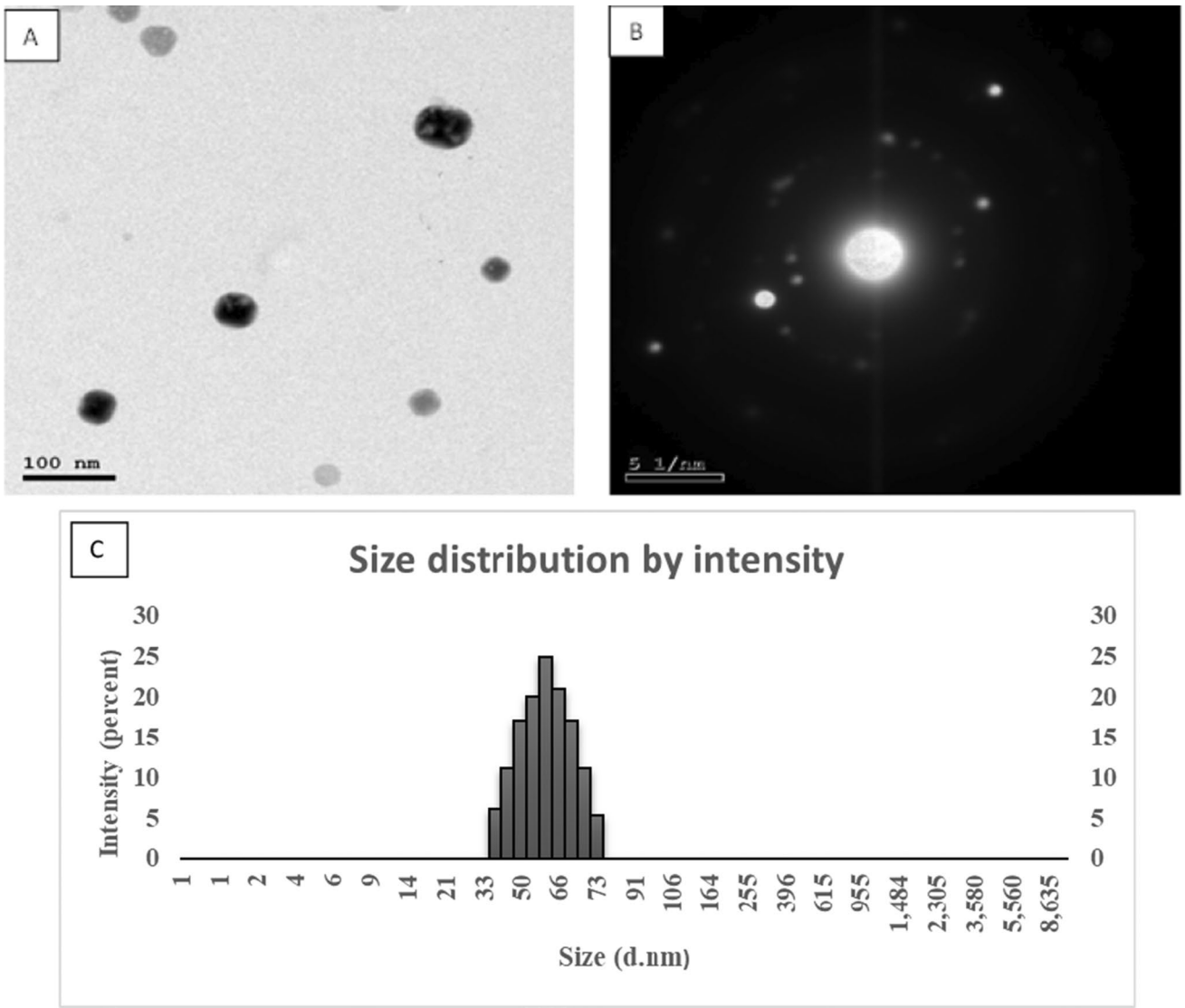

Fig. 4 Characterization of myco-synthesized SiO_2-NPs. (**A**) TEM image, (**B**) SAED pattern of SiO_2-NPs, (**C**) Dynamic light scattering system (DLS)

8.4 Physiochemical characterization of the SiO_2-NPs

The creation of nanoparticles and their shape are guaranteed by the characterization of the generated product (i.e., SiO_2-NPs). The general characteristics of nanoparticles are their size, shape, absorbance, and disparity. For the study of the nature and morphologies of nanoparticles, conventional characterization techniques, including spectroscopic and microscopic processes, are used. The size and form of a nanoparticle have a significant impact on its qualities. Advanced characterization procedures are necessary since nanoparticles are invisible to the naked eye. TEM examination was used to determine the size, shape, and morphology of the produced SiO_2-NPs. Figure 4 A; illustrates how well the metabolites in the fungal biomass filtrate stabilized the silica nanoparticles' form. The data analysis shows that the spherical forms are produced with sizes ranging from 20 to 50 nm. Using the SAED pattern, the crystalline nature of SiO_2-NPs was evaluated. Silica nanoparticles were created using an extract of *Penicillium oxalicum* as the reducing agent, and the SAED pattern showed that they were monocrystalline (Fig. 4 B). Zamani et al.'s [74] effective biosynthesis of spherical silica nanoparticles with a diameter size range of 40 to 70 nm is another noteworthy achievement. According to Rezaeian et al. [75], olive residue was used to manufacture Si-NPs with an average diameter of 30–40 nm.

Using the DLS method, the particle size of the biosynthesized SiO_2-NPs was examined (Fig. 4 C). The silica nanoparticles have an average size of 63.78 nm, according to the DLS histogram, and their poly-dispersity index (PDI), which measures their degree of mono-dispersion, was 0.265. Elella et al.'s [76] representation of the average particle size was 7 nm. As revealed by Albalawi et al. [57], the DLS and the histogram indicated an average particle size of roughly 70.1 nm with a volume of 33%.

The most popular method for examining the optical characteristics of the particles is UV–visible spectroscopy. Absorption spectroscopy in the UV–visible spectral band is referred to as UV–visible spectroscopy. The biotransformation of SiO_2-NPs was caused by the addition of *P. oxalicum* cell free extract to sodium silicate solution, as shown by the UV absorption spectra of this combination, which contain an absorption band at 280 nm (Fig. 5). and this range agrees with Biradar et al. [34], who found that the greatest absorbance was at 297 nm, which denotes the production of silica nanoparticles. Similar to this, Kannan et al. [77] reported that *Fusarium oxysporum* at 280 nm was effectively used to produce SiO_2-NPs. Other reports [78, 79] reveal an absorption band in the 240–270 nm region. The visible range absorption directly impacts how the color of the chemicals involved is seen, and in this region of the electromagnetic spectrum, molecules go through electronic transitions [34]. The biosynthesized SiO_2-NPs contained a single SPR band

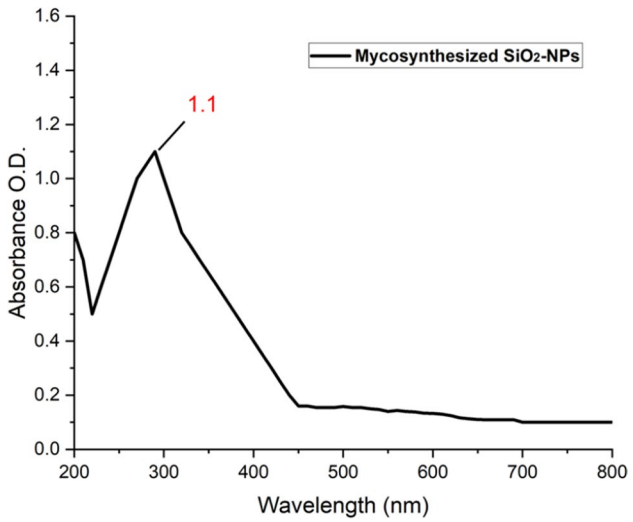

Fig. 5 UV–Vis spectroscopy of myco-synthesized SiO_2-NPs

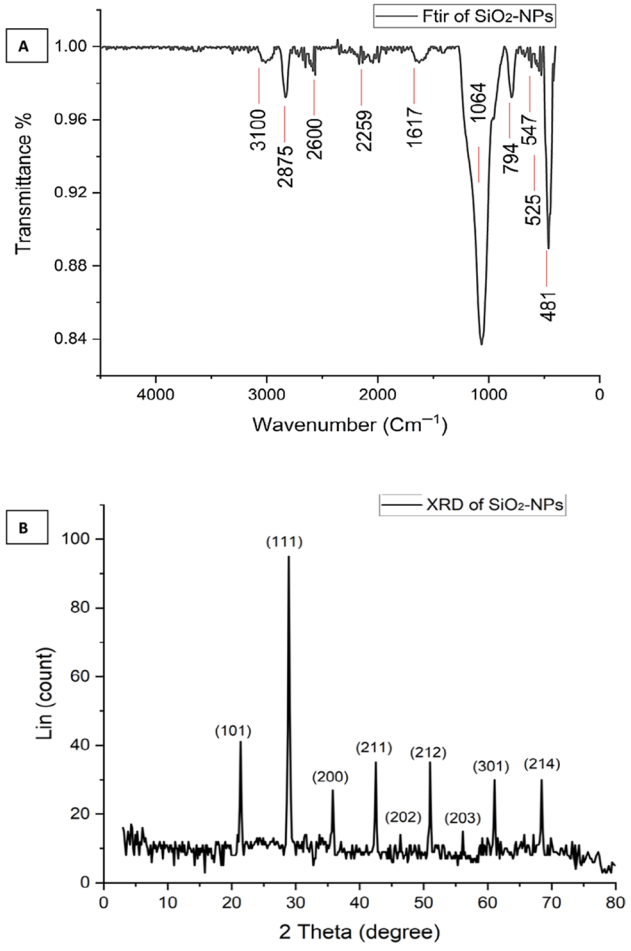

Fig. 6 (**A**) The FT-IR spectrum of myco-synthesized SiO_2-NPs; (**B**) XRD analysis of SiO_2-NPs

that was identified at a wavelength of 295 nm, according to Albalawi et al. [57]. Additionally, according to Biradar et al. [34], the greatest absorption of silicon dioxide nanoparticles is seen at 297 nm. El-Gazzar et al. [45] discovered that the formation of SiO_2-NPs took place at absorption wavelengths of about 336 nm.

Figure 6 A displays the biological SiO_2-NPs FTIR spectrum. Ten bands in the range of 3100– 411 cm^{-1} were seen in the findings. These bands are in charge of many current ensembles. A peak at 3100 cm^{-1} indicated that the alkenes and aromatics' bonds were both N–H and O–H stretching [79]. According to asymmetrical and symmetrical stretching vibrations of CH_2 groups, respectively, the bands seen at 2875, 2600, and 2259 cm^{-1} were explained [80]. The O–H stretching band on the surface of silanol groups was thought to be responsible for the band's appearance at 1617 cm^{-1} [77]. The peaks at 1064 cm^{-1}, 794 cm^{-1}, 547 cm^{-1}, 525 cm^{-1}, and 481 cm^{-1} were ascribed to the Si–O stretching vibration, Si–OH stretching vibration, Si–O-Si symmetric stretching, and Si–O-Si bending, respectively, which confirms the successful synthesis of SiO_2 nanospheres [34, 57, 81]. The adsorption of these new functional groups on the SiO_2-NPs surface plays a significant role in catalytic reactions [82]. Several studies indicated that proteins could easily bind to the NPs surface and probably act as capping stabilizing agents [83]

A significant diffraction pattern of SiO_2-NPs was found at 2 θ = 21.4°, 28.92°, 35.8°, 42.52°, 46.36°, 51.0°, 56.1°, 61.08°, and 68.44°, Fig. 6 B which matches the XRD pattern of the indices (101), (111), (200), (211), (202), (212), (203), (301), and (214), respectively. The acquired diffraction peaks confirmed the crystalline structure of SiO_2-NPs since they were the same as those reported by Albalawi et al. [57], Biradar et al. [34], and El Messaoudi et al. [70]. The Debye–Scherrer equation was used to determine the average diameter of SiO_2-NPs [84]. The SiO_2-NPs had an average crystal size of 28.79 nm, where peak position (2θ) equals 55.94 o and FWHM (2θ) equals 0.1217.

8.5 Photocatalytic degradation of crystal violet and Ribazol black b dyes by using SiO_2-NPs.

The degradation of both crystal violet and Ribazol black b dyes in water under strong UV light is used to measure the photocatalytic performance of the SiO_2 nanoparticles. The varied dye concentrations (30 and 50 mg L^{-1}) are shown versus time in Fig. 7. The decolorization of both dyes during photodegradation in the presence of SiO_2 nanoparticles was estimated using the UV–Vis spectrum. With increasing photocatalytic time, the content of both Ribazol black b and crystal violet rapidly decreased. According to Fig. 7 (A, B), at 30 mg of SiO_2 nanoparticles concentration, the Ribazol black b and CV dye degradation rose from 57% ± 1.1% and 70% ± 0.88%, respectively, to 85.1% ± 0.93% and

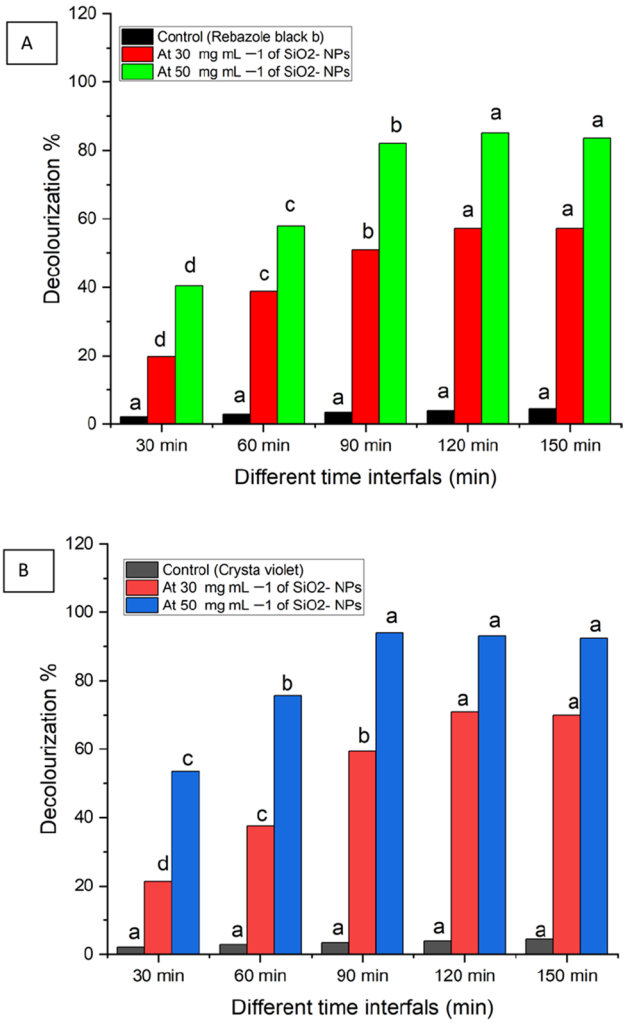

Fig. 7 (A, B). Ribazol black b and Crystal violet dyes decolourization percentages at different SiO_2-NPs concentrations 30, and 50 mg mL^{-1} at different contact time

94.1% ± 1.2%, respectively, at 50 mg of SiO_2 nanoparticles after 90 min for crystal violet and 120 min for Ribazol black b. Additionally, a time-dependent technique makes it possible to anticipate the influence of the SiO_2 nanoparticle concentration on the photodegradation of both dyes. The increase in degradation efficiency at the highest concentration of photocatalyst is notably attributed to the increased number of active sites on the surface of SiO_2 nanoparticles, which offer the highest possible active surface area for UV light absorption [85]. According to Biradar et al. [34], photodegradation of methylene blue and methyl orange (10 ppm each) with 1.5 g/dm^3 SiO_2 photocatalyst dosage achieved 98 and 95% degradation in 90 min at 25 °C with pH 7. In the best circumstances, which included 10 mg of xanthan gum/SiO_2 nanocomposite, 10 mL of MG dye (450 ppm), pH = 7, 30 C, and within 6 h, the maximum adsorption capacity was reported as 99.5% by Elella et al. [76]. Using graphene-ordered

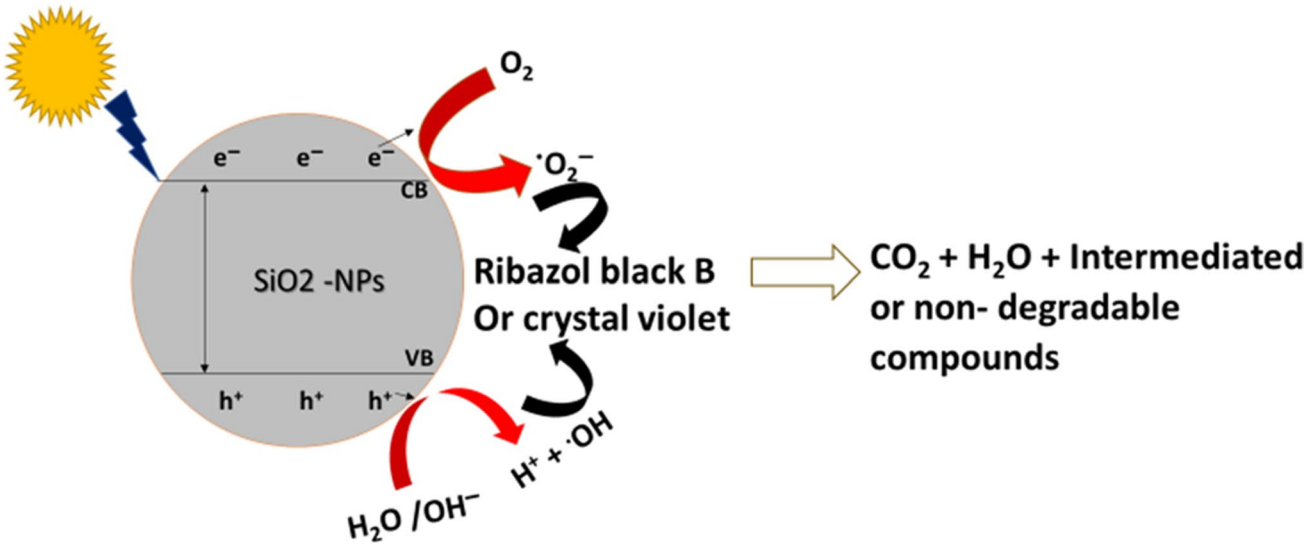

Scheme 1 Flowchart showed the mechanism used for decolourization and degradation of Crystal violet and Ribazole black b dyes by using SiO_2 nanoparticles

mesoporous silica (SBA 15)/TiO_2 nanocomposite under visible light irradiation, Ali et al. [86] reported that around 98% of MB and 89% of Tetracycline medication were photodegraded after 30 min and 60 min, respectively. For Si_2Ti, photocatalytic degradation of 90% and 85% was attained after 30 min in sunshine and UV radiation, respectively, according to Mahanta et al. [85]. Additionally, after two hours in the sun, MB deterioration reached approximately 100%. According to Huang et al. [64], who reported that Ag@Ni and Ag@Co composites showed electrifying 90.2% and 82% degradation against methyl orange (MO) by photocatalysis. Additionally, the degradation of Methylene Blue, Methyl Orange, Rhodamine-B, P-Nitroaniline, and Cresol Red dyes in the presence of I-NC catalysts following sunlight irradiation was demonstrated by Batool et al. [87] by using the green synthesized ZnO-Fe_2O_3-Co_3O_4 nanocomposite. where, Methylene Blue (99.98%) > P-Nitroaniline (99.97%) > Rhodamine-B (99.86%) > Cresol Red (99.80%) > Methyl Orange (99.6%) is the order in which the degradation efficiencies of I-NC are displayed. Furthermore, Batool et al. [88] investigate the photocatalytic activity of the MB dye degradation after 80 min by using ZnO, Fe_2O_3, and Co_3O_4 nanoparticle.

8.5.1 Possible mechanism of photocatalytic degradation

The increased dye removal in the presence of UV irradiation (photocatalysis) could be due to its impact on the exciting of the electrons from the valance band (VB) to the conductance band (CB) (Scheme 1). Once light photons are absorbed by the surface of SiO_2-NPs, the excited electrons (e −) migrate from the valence band to the conductance band, leaving holes (h^+) there (Equation (2)). Equation (3) states that the reduction process was accomplished on the CB, forming a superoxide anion ($^{\bullet}O_2^-$) via the interaction of excited e − with O_2. Equations (4) and (5) state that the as-formed O_2^- interacts with H + to form hydrogen peroxide ($HO_2^{\bullet}$), which then reacts with dissolved H^+ to generate hydrogen peroxide (H_2O_2). On the other hand, the oxidation process was achieved in VB through the reaction of h^+ with H_2O, forming highly oxidizing hydroxyl radicals ($^{\bullet}OH$) (Equations (6)). At last, different radicals began to form, attacking the dyes and breaking them down into less harmful compounds such as CO_2 and H_2O (Equations (7)) [89, 90]. Scheme 1 illustrate the proposed the photocatalytic degradation of both crystal violet and Ribazol black b dyes by using the mycosynthesized SiO_2-NPs.

$$UV - irradiation + SiO_2 - NPs \rightarrow e - + h^+ \tag{2}$$

$$e - + O_2 \rightarrow {}^{\bullet}O_{2^-} \tag{3}$$

$$O_{2^-} + H^+ \rightarrow HO_2. \tag{4}$$

$$HO_2. + H^+ \rightarrow H_2O_2 \tag{5}$$

$$h^+ + H_2O \rightarrow HO^- \tag{6}$$

$$crystalvioletorRibazolblackbdyes + radicals\left(\bullet O_{2^-}, H_2O_2, HO^-\right) \rightarrow intermediatedornon - degradablecompounds + CO2 + H2O \tag{7}$$

The role of various active species in the photocatalysis and degradation of crystal violet or Ribazol black b dyes was measured using the trapping method. As shown in Fig. 8 (A,

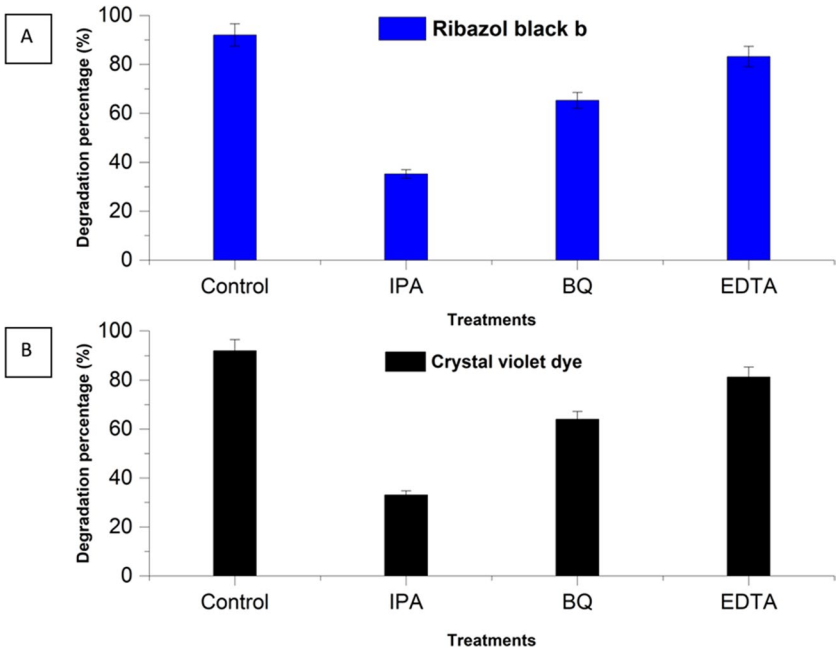

Fig. 8 **(A, B)**. The effect of the different scavengers, including isopropyl alcohol (IPA), benzoquinone (BQ), and ethylenediaminetetraacetate (EDTA) on degradation percentage of Ribazol black b and Crystal violet dyes using mycosynthesized SiO_2-NPs

B), the crystal violet or Ribazol black b degradation percentages were decreased after the addition of different free radical scavengers (IPA, QB, and EDTA) to the photocatalytic experiment. Result analysis revealed that the presence of various free radical scavengers reduced the efficacy of crystal violet or Ribazol black b degradation by SiO_2-NPs. As demonstrated, the maximum decrease in crystal violet and Ribazol black b degradation percentage was (33.1 ± 0.9%) and (35.2 ± 1.1%), respectively, which was attained due to the presence of IPA, which captured $^{\bullet}OH$. Moreover, after the addition of QB and EDTA, the degradation percentages were reduced to (64.0 ± 0.79%), (65.3 ± 1.2%) and (81.3 ± 1.2%), (83.2 ± 1.3%) for crystal violet or Ribazol black b dyes, respectively, which captured $^{\bullet}O_2^-$ and h^+. These findings showed that the addition of IPA led to the greatest decline in degradation percentages, which was then followed by the addition of EDTA and BQ. Based on the obtained data, it can be concluded that $^{\bullet}OH$ has a significant role in photocatalytic crystal violet or Ribazol black b degradation, followed by $^{\bullet}O_2^-$ and h^+.

8.5.2 Reusability and stability studies of SiO_2 nanoparticles

Under ideal circumstances, six cycles of photodegradation studies were carried out to test the stability and reusability of the NPs [91]. After the initial application, crystal violet and Ribazol black b were removed, rinsed with distilled water to remove the dye that had adhered to the surface, and then dried to remove the water content. Once more, the dried powder was used as a photocatalyst to break down the dyes. The comparison of the photodegradation and reusability of the dye's crystal violet and Ribazol black b is shown in Fig. 9 (A, B). For five cycles, there has been no discernible drop in effectiveness. After six cycles, the photodegradation efficiency reached 83% ± 1.3% for CV and 70% ± 0.9% for Ribazole black b (Fig. 9). The loss of nanoparticles to the water during the catalytic reaction and the production of intermediate materials on the photocatalyst surface are the causes of the lower performance of the photocatalytic activity during its reusability. These tests showed that the dyes crystal violet and Ribazol black b were stable and retained their photocatalytic activity throughout time. With the use of an SBA 15/TiO_2 nanocomposite, Ali et al. [86] demonstrated no discernible decline in the effectiveness of MB dye degradation over the course of seven cycles. Similar to this, Mahanta et al. [85], showed no discernible decline in Si_2Ti's ability to degrade metal after four successive cycles. Additionally, Fouda et al. [92] reported that, after ten successive batches, the ZnO-NPs produced by the *Penicillium corylophilum* strain As-1's catalytic effectiveness to degrade the MB dye dropped from 98 to 94% with a reduction percentage of 4%. Saied et al.[93] reported that thedecolorization percentages of crystal violet dye were reduced to up to 63.5% ± 1.04% when it was repeated for the fourth cycle by using Hem-NPs. Furthermore, the dye removal percentage of RR195 using ZnO@CuO-NPs/CSC nanocomposite showed removal of 82.1 ± 0.41% [94].

8.6 Bio-adsorption of heavy metals by using SiO_2 nanoparticles

Heavy metals are very harmful environmental contaminants, especially for adjacent soil, water, and aquatic creatures. Through food chains, they can reach both people and animals [95]. Heavy metal and other organic contaminant

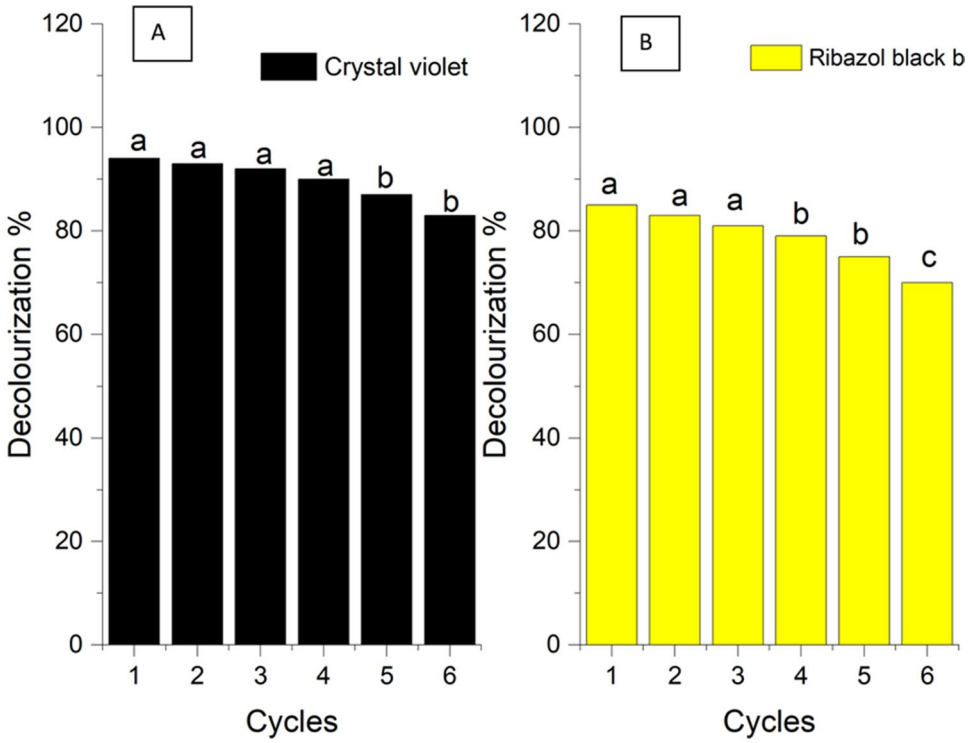

Fig. 9 **(A, B).** Reusability tests of SiO_2 nanoparticles for photocatalytic degradation of Crystal violet and Ribazole black b dyes

pollution of water and soil is seen as a serious issue that has to be resolved quickly since these pollutants have a number of adverse impacts [96]. It's interesting to note that dye effluents are the main source of heavy metal emissions into the environment. Establishing an eco-friendly mechanism for adsorbing the heavy metals before they are released into the ecosystem is therefore crucial. Because of their superior adsorption ability, non-toxicity, environmental friendliness, cheap cost, and abundance, green produced silica nanoparticles are recommended as bioadsorbents for various heavy metals [97]. The most popular and sensitive method for identifying metals and metalloids in materials is called atomic absorption spectroscopy (AAS) [98]. The most common heavy metals found in dye effluent in this investigation were cobalt (Co), lead (Pb), cadmium (Cd), and zinc (Zn), and SiO_2-NPs demonstrated a high adsorption capability toward these heavy metals. The strong adsorption ability of biosynthesized silica nanoparticles in this investigation to remove Co, Pb, Cd, and Zn with percentages of 99.9% ± 1.2%, 99.9% ± 1.3%, 99.9% ± 1.3%, and 99.4% ± 1.4%, respectively, was indicated by data analysis (Table 1). The adsorption of heavy metals onto the adsorption sites found on the NPs surface may be responsible for these elimination percentages [99]. According to Mahmoud et al. [100], reaction duration and metal concentrations were linked to the Pb adsorption rate. The greatest RE% values of 80.50% and 95.95% for Ni^{2+} and Cd^{2+}, respectively, were found at 100 ppm starting concentration, according to Gunawardhana et al. [101]. MgO and hematite NPs, on the other hand, were reported to have high removal rates of Cr by Fouda et al. [67], with MgO decreasing Cr by 87.06 and hematite NPs lowering Cr by 75.4%. Additionally, Pb, Ni, and Cd were removed by MgO-NPs at rates of 15.4%, 28.2%, and 40.6%, respectively, as opposed to 13.4%, 13.5%, and 7.3%, respectively, by hematite nanoparticles. MgO-NPs therefore outperformed α-Fe_2O_3-NPs in terms of effectiveness. At the conclusion of 48 h, remediation by Akhtar et al. [102] of Cr and Zn results in removal efficiencies of up to 67% for Cr and 55% for Zn.

Table 1 Heavy metals removal capacity due to SiO_2 nanoparticles treatments

Heavy metals	Control	After NPs treatment	Removal capacity (%)
Co (mg/L)	13.81% ± 0.51%	0.013% ± 0.35%	99.9% ± 1.2%
Pb (mg/L)	24.5% ± 1.1%	0.01% ± 071%	99.9% ± 1.3%
Zn (mg/L)	31.3% ± 1.2%	0.183% ± 1.3%	99.4% ± 1.4%
Cd (mg/L)	34.6% ± 1.12%	0.002% ± 0.73%	99.9% ± 1.3%

Data represented are means ± SD (n = 3)

8.7 Toxicity assessment

To assess the toxicity of dangerous chemicals, the seed germination assay is a sensitive, popular, quick, and efficient approach [103]. In this investigation, we employed a significant crop, maize (*Zea mays* L.), to examine the potential of SiO_2-NPs under ideal circumstances (50.0 mg mL^{-1} /90 min/sunlight for crystal violet and 50.0 mg mL^{-1} /120 min/sunlight for Ribaol black b) in dye treatments in comparison to dyes without any treatments. According to the data that was assessed (Fig. 10), the silica nanoparticles treatment significantly reduces the toxicity of dye effluents. Analysis of variance revealed that, when treated CV and Ribazole black b effluents were used, the root length of corn rose by (28 ± 0.35) and (21 ± 0.51) cm, respectively, as compared to untreated effluents. Additionally, dye effluents that have not been treated are extremely hazardous to maize shoot length and did not cause any growth responses (Fig. 10). It's interesting to see that there is a difference between corn watered with tap water and maize irrigated with effluents treated by NPs in terms of shoot length. The residual salts, organic residues, and other contaminants may be to blame for the reduction in root length watered by effluents treated by NPs as compared to tap water [104]. To evaluate the effectiveness at the gene level, more research is needed to complete the phytotoxicity and genotoxicity studies. The information gathered leads to the conclusion that environmentally friendly synthetic silica nanoparticles are a viable tool for reducing the toxicity of textile wastewater and tannery effluents through the conversion of harmful pollutants into safe products or by the adsorption of heavy metals from aqueous solutions. The phytotoxicity of maize and broad beans grown under textile and tannery effluent irrigation was investigated by Fouda et al. [52] both before and after MgO-NPs treatment. The treated MB dye-solution-irrigated *Vicia faba* exhibited excellent germination, as demonstrated by Saied et al. [104].

8.8 Assessing the impact of CV and Ribazol black b solutions on *Zea mays* growth

Besides seed germination, the toxicity of dyes and their biodegradable products were also investigated through the growth performance of the *Zea mays* plant in the soil (Fig. 11). Root lengths of maize treated with distilled water and biodegradable materials measured 33.0 ± 0.76 cm, $28.0 \pm 0.35$and 21.0 ± 0.51cm, respectively, which significantly differed from those treated with dyes (7.0 ± 0.24, 5.4 ± 0.41 and 4.0 ± 0.62 cm), as indicated by data analysis. On the other hand, a noteworthy difference ($p \leq 0.05$) was observed when comparing the shoot length of seeds irrigated with crystal violet treated with SiO_2 nanoparticles (88.0 ± 0.45 cm), Ribazol black b treated with SiO_2 nanoparticles (57.0 ± 0.32 cm), and seeds irrigated with tap water (100.0 ± 0.54 cm) (Fig. 11). The growth performances of *Zea mays* varied according to different treatments. It is

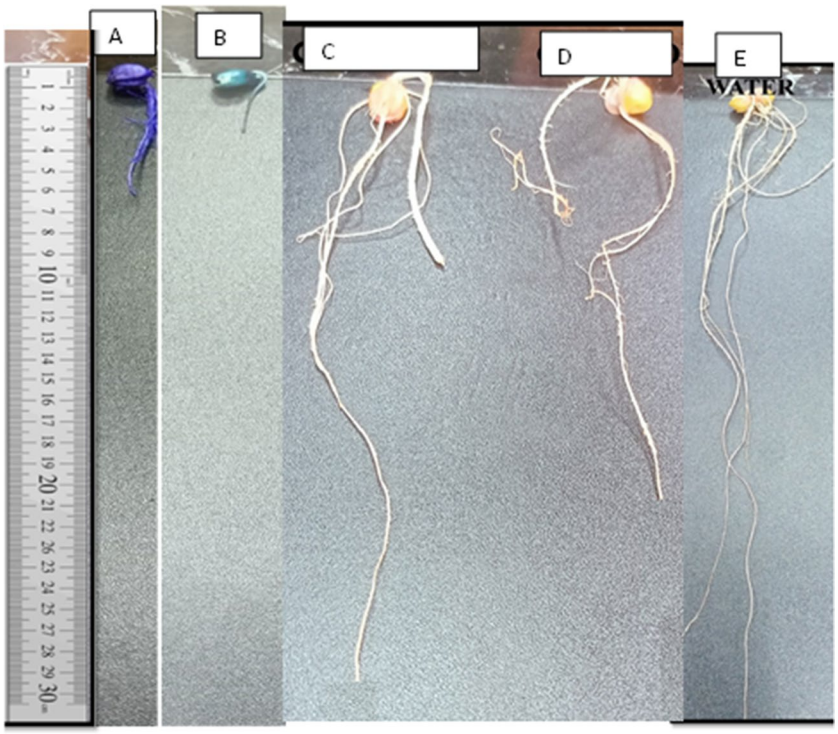

Fig. 10 Toxicity assessment of CV and Ribazole black b effluent before and after nanoparticles treatments compared with distilled H_2O on *Zea mays* plant. Panel (A, B) Control without any treatment; panel;(C, D), products of CV and Ribazole black b after nanoparticles treatments; (E) *Zea mays* plant irrigated by tap water

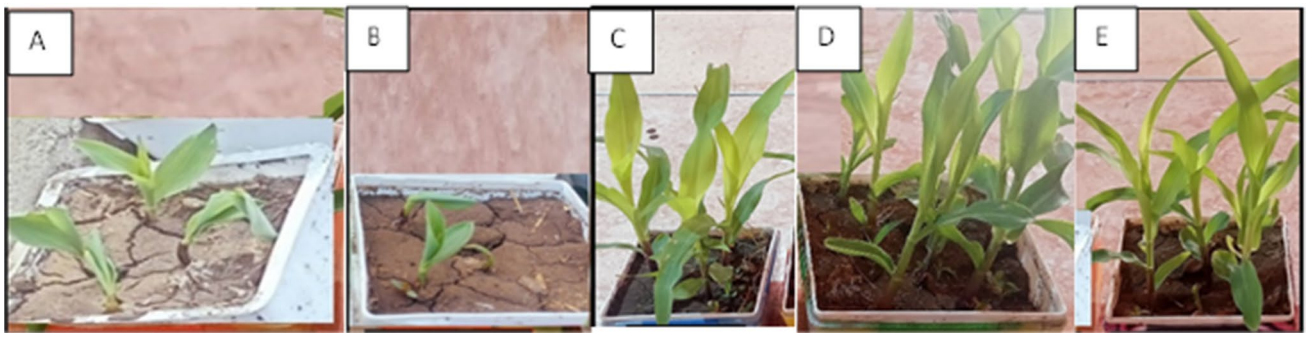

Fig. 11 Greenhouse Experiment of CV and Ribazole black b effluent before and after nanoparticles treatments compared with tap water on *Zea mays* plant. Panel (A, B) Control without any treatment; panel;(C, D), products of CV and Ribazole black b after nanoparticles treatments; (E) *Zea mays* plant irrigated by tap water

suggested that the toxicity of dyes after biodegradation using NPs was decreased as compared with their toxicity before NPs degradation [105].

9 Conclusion

Nanoparticles are being synthesized using chemical and physical methods; however, the adverse effects of these methods have led tothe discovery of novel sustainable methods. The microbial-mediated synthesis of SiO_2-NPs exhibits a greater advantage over other conventional techniques as it produces a uniform, spherical shaped nanoparticle. The biogenic synthesis of SiO_2-NPs was achieved through an extracellular method using a cell-free filtrate of endophytic *P. oxalicum*, which led to the production of spherical nanoparticles within the size range of 20 to 50 nm. FTIR measurement provided strong evidence for the presence of proteins and functional groups that stabilize and prevent the agglomeration of the particles. Synthesized nanoparticles were found to be capable of photocatalytic crystal violet and Ribazol black b dye degradation. Silica nanoparticles showed the maximum enhancement in photocatalytic activity of dyes 94.1% and 85.1%, respectively. The SiO_2-NPs exhibited high adsorption capabilities for heavy metals, making them promising bioadsorbents for the eco-friendly removal of these pollutants, which remove Co, Pb, Cd, and Zn with percentages of 99.9%, 99.9%, 99.9%, and 99.4%, respectively. Furthermore, the study evaluated the phytotoxicity effects of SiO_2-NPs on *Zea mays* and found that NPs biodegradation led to reduced toxicity compared to untreated dyes, whose root length increased to 28 and 21 cm, respectively, when treated with CV and Ribazole black b effluents.

Supplementary Information The online version contains supplementary material available at https://doi.org/10.1007/s13399-024-05350-6.

Authors contributions **H.E.A**.: Formal analysis, Investigation, methodology, Resources, Software; Writing-original draft; **E.S.**: Conceptualization, Data curing, Formal analysis, Investigation, methodology, Project adminstration, Resources, Software, Validation, Visualization, Writing-original draft, Writing -review and editing.**; S.H.:** Conceptualization, Data curing, Formal analysis, Investigation, methodology, Project adminstration, Resources, Software, Validation, Visualization, Writing-original draft, Writing -review and editing; **H.M.M.:** Conceptualization, Investigation, Project adminstration, Supervision, Visualization, Validation**; M.H.S**.: Conceptualization, Data curing, Formal analysis, Investigation, methodology, Project adminstration, Resources, Software, Validation, Visualization, Writing-original draft, Writing -review and editing.

Funding Open access funding provided by The Science, Technology & Innovation Funding Authority (STDF) in cooperation with The Egyptian Knowledge Bank (EKB).

Data availability The data used to support the findings of this study are available from the corresponding author upon request.

Declarations

Ethical approval There are no experiments that require ethical approval.

Competing interests This work does not include any interests of a financial or personal nature.

References

1. Mughal B et al. (2021) Biogenic nanoparticles: Synthesis, characterisation and applications. 11(6): 2598
2. Kumari M et al. (2023) Nanotechnology for Bioremediation of Industrial Wastewater Treatment, in Advanced Application of Nanotechnology to Industrial Wastewater. Springer. 105-131
3. Priyadarshini E et al. (2021) Metal-Fungus interaction: Review on cellular processes underlying heavy metal detoxification and synthesis of metal nanoparticles. **274**: 129976
4. Sidhu, A.K., N. Verma, and P.J.F.i.N. Kaushal, *Role of biogenic capping agents in the synthesis of metallic nanoparticles and evaluation of their therapeutic potential.* 2022. **3**: p. 801620.
5. Uddin FJC (2021) Environmental hazard in textile dyeing wastewater from local textile industry. **28**(17): 10715-10739
6. Yildirim, O.A., M. Bahadir, and E.J.F.-F.E.B. Pehlivan, *Detrimental effects of commonly used textile dyes on the aquatic environment and human health–a review.* 2022(9329): p. 33–41.
7. Lyu F et al. (2023) A novel framework for water accounting and auditing for efficient management of industrial water use. **395**: 136458
8. Ajiboye TO, Oyewo OA, Onwudiwe DCJC (2021) Simultaneous removal of organics and heavy metals from industrial wastewater: A review. **262**: 128379
9. Siddiqui N, Dahiya P (2023) Key role of microorganisms in industrial wastewater treatment, in Development in Wastewater Treatment Research and Processes. Elsevier. p. 31-47
10. Mitiku AAJIJPSRR (2020) A review on water pollution: causes, effects and treatment methods. **60**(2): 94–101
11. Nahiun KM et al. (2021) A review on the methods of industrial waste water treatment. **7**(3): 20-31
12. Boudjabi S, Ababsa N, Chenchouni H (2023) Sewage and sewage treatment, in The Palgrave Handbook of Global Sustainability. Springer. 719-745
13. Nachiyar CV et al. (2023) Developments in treatment technologies of dye-containing effluent: A review 100339
14. Shoaib M et al. (2022) Biological methods for degradation of textile dyes from textile effluent, in Development in Wastewater Treatment Research and Processes. Elsevier. 329-353
15. Rasheed T et al (2020) Surfactants-based remediation as an effective approach for removal of environmental pollutants—A review. 318: 113960
16. Varjani S et al (2020) *Treatment of wastewater from petroleum industry: current practices and perspectives.* 27: 27172-27180
17. Morin-Crini N et al (2022) Removal of emerging contaminants from wastewater using advanced treatments. A review. **20**(2): 1333-1375
18. Shabir M et al (2022) A review on recent advances in the treatment of dye-polluted wastewater. **112**: 1-19
19. Rajoria S et al (2022) Treatment of electroplating industry wastewater: a review on the various techniques. **29**(48): 72196-72246
20. Hairom NHH et al (2021) A review of nanotechnological applications to detect and control surface water pollution. **24**: 102032
21. Qamar SUR, Ahmad JNJJoML (2021) Nanoparticles: Mechanism of biosynthesis using plant extracts, bacteria, fungi, and their applications. 334: 116040
22. Salem SS, Fouda A.J.B.t.e.r (2021) Green synthesis of metallic nanoparticles and their prospective biotechnological applications: an overview. 199: 344–370
23. Hasanien YA et al (2023) Green synthesis of SiO2 nanoparticles from Egyptian white sand using submerged and solid-state culture of fungi. 1–14
24. Ilahi N et al (2022) Biosynthesis of silver nanoparticles using endophytic Fusarium oxysporum strain NFW16 and their in vitro antibacterial potential. 2023(4): 1568–1579
25. Mohana S, Sumathi SJJoCS (2020) Multi-functional biological effects of palladium nanoparticles synthesized using Agaricus bisporus. 31: 391–400
26. Clarance P et al. (2020) Green synthesis and characterization of gold nanoparticles using endophytic fungi Fusarium solani and its in-vitro anticancer and biomedical applications. **27**(2): 706-712
27. Boulkhessaim S et al. (2022) Emerging trends in the remediation of persistent organic pollutants using nanomaterials and related processes: A review. **12**(13): 2148
28. Ahmed SF et al. (2022) Nanomaterials as a sustainable choice for treating wastewater. **214**: 113807
29. Wareing TC, Gentile P, Phan A.N.J.A.n (2021) Biomass-based carbon dots: current development and future perspectives. 15(10): 15471–15501
30. Lu F, Astruc DJCCR (2020) Nanocatalysts and other nanomaterials for water remediation from organic pollutants. 408 213180
31. López M et al. (2020) Hydrodeoxygenation of guaiacol into cyclohexane over mesoporous silica supported Ni–ZrO2 catalyst. 309: 110452
32. Hanif A et al. (2019) Silica supported MgO as an adsorbent for precombustion CO2 capture. 2(10): 6565–6574
33. Wiśniewska M et al. (2020) Alumina-silica-titania adsorbent for hazardous azo and phtalocyanine dyes removal from textile baths and wastewaters–the impact of ionic surfactants. 56
34. Biradar AI et al. (2021) Photocatalytic degradation of dyes using one-step synthesized silica nanoparticles. 43: 2832-2838
35. September LA et al. (2023) Green synthesis of silica and silicon from agricultural residue sugarcane bagasse ash–a mini review. 13(2): 1370–1380
36. Pieła A et al. (2020) Biogenic synthesis of silica nanoparticles from corn cobs husks. Dependence of the productivity on the method of raw material processing. 99: 103773
37. Nidheesh PV et al. (2022) Treatment of textile wastewater by sulfate radical based advanced oxidation processes. 293: 121115
38. Verma A et al. (2022) Investigation on structural and optical properties of porous SnO2 nanomaterial fabricated by direct liquid injection chemical vapour deposition technique. 348: 114723
39. Singh S et al. (2019) Applications of nanoparticles in wastewater treatment. 395–418
40. Fouda AH et al. (2015) Biotechnological applications of fungal endophytes associated with medicinal plant Asclepias sinaica (Bioss.). 60(1): 95–104
41. Pitt JIJM (1979) Penicillium crustosum and P. simplicissimum, the correct names for two common species producing tremorgenic mycotoxins. 71(6): 1166–1177
42. Visagie C et al. (2014) Identification and nomenclature of the genus Penicillium. 78(1): 343-371
43. White TJ et al. (1990) Amplification and direct sequencing of fungal ribosomal RNA genes for phylogenetics. 18(1): 315-322
44. Gholami-Shabani M et al. (2021) Mycosynthesis and physicochemical characterization of vanadium oxide nanoparticles using the cell-free filtrate of fusarium oxysporum and evaluation of their cytotoxic and antifungal activities. **2021**: 1-12
45. El-Gazzar N et al. (2021) Assessment the using of silica nanoparticles (SiO2NPs) biosynthesized from rice husks by Trichoderma harzianum MF780864 as water lead adsorbent for immune status of Nile tilapia (Oreochromis niloticus). 28(9): 5119–5130
46. Hassan SE-D et al. (2021) Rhizopus Oryzae-mediated green synthesis of magnesium oxide nanoparticles (MgO-NPs): A

promising tool for antimicrobial, mosquitocidal action, and tanning effluent treatment. 7(5): 372
47. Ateeb M et al. (2023) Photocatalytic and Antibacterial activities of bio-synthesised silver nanoparticles (AgNPs) using Grewia asiatica leaves extract. 1–19
48. Hashem AH, Salem SSJBj (2022) Green and ecofriendly biosynthesis of selenium nanoparticles using Urtica dioica (stinging nettle) leaf extract: Antimicrobial and anticancer activity. 17(2): 2100432
49. Muhiuddin G et al. (2023) Synthesis of Ni doped barium hexaferrite by microemulsion route to enhance the visible light-driven photocatalytic degradation of crystal violet dye. 49(3): 4342-4355
50. Fouda A et al. (2023) Green Synthesis of Zinc Oxide Nanoparticles Using an Aqueous Extract of Punica granatum for Antimicrobial and Catalytic Activity. 14(4): 205
51. Malik LA et al. (2019) Detection and removal of heavy metal ions: a review. **17**: 1495-1521
52. Fouda, A., et al., *Photocatalytic degradation of real textile and tannery effluent using biosynthesized magnesium oxide nanoparticles (MgO-NPs), heavy metal adsorption, phytotoxicity, and antimicrobial activity.* 2021. **9**(4): p. 105346.
53. Abo-Elyousr KA et al. (2022) Management of cumin wilt caused by Fusarium oxysporum using native endophytic bacteria. **12**(10): 2510
54. Pandey S et al. (2022) Effect of different solutions on seed germination and growth of different species of seeds-review. 1(2): 168-172
55. Sahu PK et al. (2022) Surface sterilization for isolation of endophytes: Ensuring what (not) to grow. 62(6): 647–668
56. Tsivileva O, Pozdnyakov A, Ivanova AJM (2021) Polymer nanocomposites of selenium biofabricated using fungi. 26(12): 3657
57. Albalawi MA et al. (2022) Mycosynthesis of silica nanoparticles using aspergillus niger: control of Alternaria solani causing early blight disease, induction of innate immunity and reducing of oxidative stress in eggplant. 11(12): 2323
58. Barabadi H et al. (2019) Penicillium family as emerging nanofactory for biosynthesis of green nanomaterials: a journey into the world of microorganisms. 30: 843-856
59. Hashem AH et al. (2021) Biomedical applications of mycosynthesized selenium nanoparticles using Penicillium expansum ATTC 36200. 1–11
60. Annamalai J et al. (2021) Recent trends in microbial nanoparticle synthesis and potential application in environmental technology: a comprehensive review. 28: 49362-49382
61. Yamini V, Rajeswari VDJJEN (2023) Effective bio-mediated nanoparticles for bioremediation of toxic metal ions from wastewater–A review. 12(2): 12–33
62. Muzahid ANM et al. (2023) Potentials of mycosynthesized nanomaterials for efficient remediation of environmental contaminants, in Fungal Cell Factories for Sustainable Nanomaterials Productions and Agricultural Applications. Elsevier. 693-724
63. Huang X et al. (2023) Investigation of pretreatment parameters for bioethanol production from Spirogyra using ZnO nanoparticles. 1–11
64. Huang X et al. (2023) Biological synthesis of bimetallic hybrid nanocomposite: a remarkable photocatalyst, adsorption/desorption and antimicrobial agent. 17: 100446
65. Hussain R et al. (2023) Casting zinc oxide nanoparticles using Fagonia blend microbial arrest. 195(1): 264-282
66. A Abd Elmohsen S et al. (2019) Green synthesis, Optimization and Characterization of SiO2 nanoparticles using Aspergillus tubingensis F20 isolated from drinking water. 3(6): 546–557
67. Fouda A et al. (2021) Catalytic degradation of wastewater from the textile and tannery industries by green synthesized hematite (α-Fe2O3) and magnesium oxide (MgO) nanoparticles. 3: 29–41
68. Saied E et al. (2021) The catalytic activity of biosynthesized magnesium oxide nanoparticles (MgO-NPs) for inhibiting the growth of pathogenic microbes, tanning effluent treatment, and chromium ion removal. 11(7): 821
69. Otari SV et al. (2019) Biomolecule-entrapped SiO2 nanoparticles for ultrafast green synthesis of silver nanoparticle–decorated hybrid nanostructures as effective catalysts. 45(5): 5876–5882
70. El Messaoudi N et al. (2022) Biosynthesis of SiO2 nanoparticles using extract of Nerium oleander leaves for the removal of tetracycline antibiotic. 287: 132453
71. Cai W et al. (2020) Modified green synthesis of Fe3O4@ SiO2 nanoparticles for pH responsive drug release. 112: 110900
72. Miu BA, Dinischiotu AJM (2022) New Green Approaches in Nanoparticles Synthesis: An Overview. 27(19): 6472
73. El-Belely EF et al. (2021) Green synthesis of zinc oxide nanoparticles (ZnO-NPs) using Arthrospira platensis (Class: Cyanophyceae) and evaluation of their biomedical activities. 11(1): 95
74. Zamani H et al. (2020) Biosynthesis of silica nanoparticle using Saccharomyces cervisiae and its application on enhanced oil recovery. 190: 107002
75. Rezaeian M et al. (2021) Green synthesis of silica nanoparticles from olive residue and investigation of their anticancer potential. 16(18): 1581-1593
76. Elella MHA et al. (2021) Green antimicrobial adsorbent containing grafted xanthan gum/SiO2 nanocomposites for malachite green dye. 191: 385–395
77. Kannan M et al. (2015) Biobased approach for the synthesis, characterization, optimization and application of silica nanoparticles by fungus Fusarium oxysporum. 2: 223–233
78. Nakamae K et al. (2021) Thermally stable high-contrast iridescent structural colours from silica colloidal crystals doped with monodisperse spherical black carbon particles. **2**(18): 5935-5941
79. El-Saadony MT et al. (2021) Biological silicon nanoparticles improve Phaseolus vulgaris L. yield and minimize its contaminant contents on a heavy metals-contaminated saline soil. 106: 1–14
80. Sharma P et al. (2023) A novel and facile green synthesis of SiO2 nanoparticles for removal of toxic water pollutants. 13(1): 735–747
81. Ramya E et al. (2019) CuO@ SiO2 nanoparticles assisted photocatalytic degradation of 4-nitrophenol and their antimicrobial activity studies. 12: 100240
82. Nayl A et al. (2022) Recent progress in the applications of silica-based nanoparticles. 12(22): 13706-13726
83. Rana A, Yadav K, Jagadevan SJJoCP (2020) A comprehensive review on green synthesis of nature-inspired metal nanoparticles: Mechanism, application and toxicity. 272: 122880
84. Chatterjee A et al. (2023) Photodegradation of toxic Malachite Green dye by ZnO and ZnO/SiO2 nanocomposites under Solar Radiation–a green practice
85. Mahanta U, Khandelwal M, A.S.J.A.S.S. Deshpande (2022) TiO2@ SiO2 nanoparticles for methylene blue removal and photocatalytic degradation under natural sunlight and low-power UV light. 576: 151745
86. Ali A et al. (2021) Enhanced photocatalytic degradation of antibiotic drug and dye pollutants by graphene-ordered mesoporous silica (SBA 15)/TiO2 nanocomposite under visible-light irradiation. 324: 114696
87. Batool S et al. (2022) Green synthesized ZnO-Fe2O3-Co3O4 nanocomposite for antioxidant, microbial disinfection and degradation of pollutants from wastewater. 105: 104535
88. Batool S et al. (2022) Green synthesis of Cordia myxa incubated ZnO, Fe2O3, and Co3O4 nanoparticle: Characterization, and their response as biological and photocatalytic agent. 33(11): 103780

89. Selvaraj V et al. (2021) An over review on recently developed techniques, mechanisms and intermediate involved in the advanced azo dye degradation for industrial applications. 1224: 129195
90. Som I, Roy M, Saha RJC (2020) Advances in Nanomaterial-based Water Treatment Approaches for Photocatalytic Degradation of Water Pollutants. 12(13): 3409-3433
91. Wouters RD et al. (2023) Zinc oxide nanoparticles: Biosynthesis, characterization, biological activity and photocatalytic degradation for tartrazine yellow dye. 371: 121090
92. Fouda A et al. (2020) Optimization of green biosynthesized visible light active CuO/ZnO nano-photocatalysts for the degradation of organic methylene blue dye. 6(9)
93. Saied E et al. (2022) Mycosynthesis of hematite (α-Fe2O3) nanoparticles using Aspergillus niger and their antimicrobial and photocatalytic activities. 9(8): 397
94. Hasanin MS et al. (2023) A novel nanocomposite based on mycosynthesized bimetallic copper-zinc nanoparticles, nanocellulose and chitosan: Characterization, antimicrobial and photocatalytic activities
95. Sonone SS et al. (2020) Water contamination by heavy metals and their toxic effect on aquaculture and human health through food Chain. 10(2): 2148-2166
96. Rajendran S et al. (2022) A critical review on various remediation approaches for heavy metal contaminants removal from contaminated soils. 287: 132369
97. Singh NB, Susan B, Guin M.J.C.P.B (2021) Applications of green synthesized nanomaterials in water remediation. 22(6): 733–761
98. Mohammed AMJEJoE, Research T (2021) Elemental analysis using atomic absorption spectroscopy. 6(7): 48–51
99. Almomani F et al. (2020) Heavy metal ions removal from industrial wastewater using magnetic nanoparticles (MNP). 506: 144924
100. Mahmoud AED et al. (2021) Green copper oxide nanoparticles for lead, nickel, and cadmium removal from contaminated water. 11(1): 12547
101. Gunawardhana B et al. (2020) Synthesis of hematite nanodiscs from natural laterites and investigating their adsorption capability of removing Ni2+ and Cd2+ ions from aqueous solutions. 4(2): 57
102. Akhtar FZ et al. (2020) Remediation of heavy metals (Cr, Zn) using physical, chemical and biological methods: a novel approach. 2: 1–14
103. Balestri E et al. (2019) Phytotoxicity assessment of conventional and biodegradable plastic bags using seed germination test. 102: 569-580
104. Saied E et al. (2022) Photocatalytic and antimicrobial activities of biosynthesized silver nanoparticles using Cytobacillus firmus. 12(9): 1331
105. Narasaiah BP, B.K.J.J.o.S.C.S. Mandal (2020) Remediation of azo-dyes based toxicity by agro-waste cotton boll peels mediated palladium nanoparticles. 24(2): 267–281